A Study of Solar Flare Effects on the Geomagnetic Field Components during Solar Cycles 23 and 24

Oswald Didier Franck Grodji, Vafi Doumbia, Paul Obiakara Amaechi, Kassamba Abdel Aziz Diaby, Paul Obiakara Amaechi, Christine Amory-Mazaudier, Kouassi N'guessan, Kassamba Abdel Aziz Diaby, Tuo Zie, Kouadio Boka

atmosphere

MDPI

Article

A Study of Solar Flare Effects on the Geomagnetic Field Components during Solar Cycles 23 and 24

Oswald Didier Franck Grodji [1,*], Vafi Doumbia [1,*], Paul Obiakara Amaechi [2,3,*], Christine Amory-Mazaudier [4,5,6], Kouassi N'guessan [1], Kassamba Abdel Aziz Diaby [1], Tuo Zie [1] and Kouadio Boka [1]

1 Laboratoire de Physique de l'Atmosphère, UFR-SSMT, Université Félix Houphouët BOIGNY, Abidjan 01 BPV 34, Côte d'Ivoire; nguessank23@yahoo.fr (K.N.); diabyaziz@yahoo.fr (K.A.A.D.); zietuo@hotmail.fr (T.Z.); bokak2@yahoo.fr (K.B.)
2 Department of Physics, University of Lagos, Lagos 101017, Nigeria
3 Department of Physical Sciences, Chrisland University, Abeokuta 110001, Nigeria
4 Laboratoire de Physique des Plasmas, Pierre and Marie Curie University, UPMC Paris 6, F-75005 Paris, France; christine.amory@lpp.polytechnique.fr
5 Laboratoire de Physique des Plasmas, Sorbonne Universités, F-75005 Paris, France
6 International Centre for Theoretical Physics, T/ICT4D, ICTP, Stradacostiera, 11, I-34151 Trieste, Italy
* Correspondence: franckgrodji@yahoo.fr (O.D.F.G.); vafid@yahoo.fr (V.D.); paoloobiaks@yahoo.fr (P.O.A.)

Abstract: In this paper, we investigated the impact of solar flares on the horizontal (H), eastward (Y) and vertical (Z) components of the geomagnetic field during solar cycles 23 and 24 (SC23/24) using data of magnetometer measurements on the sunlit side of the Earth. We examined the relation between sunspot number and solar flare occurrence of various classes during both cycles. During SC23/24, we obtained correlation coefficient of 0.93/0.97, 0.96/0.96 and 0.60/0.56 for C-class, M-class and X-class flare, respectively. The three components of the geomagnetic field reached a peak a few minutes after the solar flare occurrence. Generally, the magnetic crochet of the H component was negative between the mid-latitudes and Low-latitudes in both hemispheres and positive at low latitudes. By contrast, the analysis of the latitudinal variation of the Y and Z components showed that unlike the H component, their patterns of variations were not coherent in latitude. The peak amplitude of solar flare effect (sfe) on the various geomagnetic components depended on many factors including the local time at the observing station, the solar zenith angle, the position of the station with respect to the magnetic equator, the position of solar flare on the sun and the intensity of the flare. Thus, these peaks were stronger for the stations around the magnetic equator and very low when the geomagnetic field components were close to their nighttime values. Both cycles presented similar monthly variations with the highest sfe value (ΔH_{sfe} = 48.82 nT for cycle 23 and ΔH_{sfe} = 24.68 nT for cycle 24) registered in September and lowest in June for cycle 23 (ΔH_{sfe} = 8.69 nT) and July for cycle 24 (ΔH_{sfe} = 10.69 nT). Furthermore, the sfe was generally higher in cycle 23 than in cycle 24.

Keywords: solar flares; solar flare effect; geomagnetic components; latitude variation

Citation: Grodji, O.D.F.; Doumbia, V.; Amaechi, P.O.; Amory-Mazaudier, C.; N'guessan, K.; Diaby, K.A.A.; Zie, T.; Boka, K. A Study of Solar Flare Effects on the Geomagnetic Field Components during Solar Cycles 23 and 24. *Atmosphere* **2022**, *13*, 69. https://doi.org/10.3390/atmos13010069

Academic Editor: Sergey Pulinets

Received: 30 November 2021
Accepted: 27 December 2021
Published: 31 December 2021

1. Introduction

The sun is a powerful star and the primary source of energy on the Earth. The dynamics of the sun's magnetic field is primarily governed by internal dynamo processes which can be quite sporadic in nature. Activities on the sun can significantly affect the environment of all planets in the solar system, particularly Earth's atmosphere. These include solar flares, coronal mass ejections, solar wind, proton events and the emission of gamma rays which can substantially change the magnetic, chemical and electrical status of the geospace environment, thus affecting the Global Navigation Satellite System (GNSS) which has now found diverse applications in various fields. This study focused on the electromagnetic interactions and the related changes in the geomagnetic field during solar flares.

Solar flares (SFs) are sudden releases of huge amounts of energy from the sun toward our planet with significant increase in extreme ultraviolet (EUV) and X-ray fluxes during a short period [1]. SFs are a significant component of space weather; the others being Coronal Mass Ejection (CMEs), the solar wind speed and the Corotating Interactions Regions (CIRs) including the ensuing geomagnetic storms. CMEs are explosive ejections of plasma (electrons, protons and helium ions) from the solar corona. Studies have, however, shown that CMEs and solar proton events (SEPs) are often associated with solar flare events [2–4].

The Geostationary Operational Environmental Satellites (GOES) of the National Oceanic and Atmospheric Administration (NOAA) started solar soft X-ray observations in 1976 [5]. The GOES measures X-ray fluxes in the wavelength range of λ = 0.1–0.8 nm. These observations are useful in the classification of solar flares according to their intensity. Solar flares are thus classified using the letters A, B, C, M and X depending on their X-ray peak flux in the wavelength range from 0.1 to 0.8 nm. X class flares are major events with very intense luminosity and a large amount of X-ray flux in the order of 10^{-4} W.m^{-2}. M class flares are less bright with X-flux greater than 10^{-5} W.m^{-2}; they are capable of inducing hard electromagnetic emissions and radio emission (solar radio bursts), which affect low-orbital spacecraft and ISS [6]. They can also interfere with satellite radio signals and GPS navigation signals. The other classes (A–C) which are low in luminosity with little effect on the Earth's ionosphere will be briefly mentioned, but not analyzed in the present work.

Solar electromagnetic emissions from SFs ranging from gamma rays to X-rays are sources of sudden ionization in the Earth's ionosphere. Enhanced X-ray fluxes during the flare are known to cause increased ionization in the Earth's lower ionosphere [7]. This alteration of the ionospheric electron density profile is known as Sudden Ionospheric Disturbances (SID) [8]. When SFs are emitted, they interact with the Earth's ionosphere by increasing its conductivity. Furthermore, additional currents are generated in the Earth's ionosphere during flare and their signatures appear as a magnetic crochet otherwise known as Solar Flare Effect (sfe). This signature is observed on magnetograms approximately few minutes after the beginning of SFs [9]. The first discovery of sfe on the geomagnetic field was made by [10], who simultaneously observed bright chromospheric eruptions by a telescope on September 1, 1859, and the appearance of a geomagnetic crochet on magnetograms. Analyzing the effects of solar flare in 18 magnetic stations in Western Europe, America and the Pacific [11] showed that geomagnetic sfes manifested as an increase in the daily variation (Sq) over the sunlit hemisphere, which was thought to be due to the increased of atmospheric ionization by UV radiation from the SFs. They also showed that the fading of radio waves is due to an increase in ionization in the D-region of the ionosphere. They further found that the upper regions of the ionosphere were not affected by the SFs. Subsequently, sfes have been the subject of several studies (see, e.g., in [12–18]). The authors of [19] have shown that one of the main reasons for further study of the solar flare dynamics is that these explosions can interfere with the GPS and communication systems. The authors of [20] observed two types of sfes at Ebre: the regular and reversed sfe. They noticed that the reversed sfes are not a rare or a sporadic phenomenon but that they occur frequently. Reversed sfes appear mostly in the hours before local noon and especially at equinox and correlate with solar activity more weakly than regular sfes. Moreover, these flares are essential for understanding space weather [19].

The objective of this work is to investigate the effect of SFs on the Earth's magnetic field at the mid and low latitudes. For this purpose, we examined SFs in the sunlit part of the Earth during solar cycles 23 and 24 and analyzed their impact on the geomagnetic field components recorded in all stations during the flares. We further characterized the flare effect on the geomagnetic components with respect to latitude, solar zenith angle and season of occurrence of the flare. The second section presents the data and methods while the third one gives the results. The discussion and conclusion are presented in Sections 4 and 5, respectively.

2. Data and Methods

2.1. GOES Satellite Data

Between 1996 and 2018, a large number of solar flares (SFs) were produced on the sun, and their effects were felt in all longitudinal sectors on the Earth. The SFs were selected from GOES archives available at www.spaceweatherlive.com/fr/archive.html, accessed on 1 November 2021. The selection was based on the geographical position of the active region (AR) from which the flare was emitted with respect to the Earth. We equally obtained X-ray flux data in the wavelength band of 0.1–0.8 Â from GOES8 (https://www.ngdc.noaa.gov/stp/satellite/goes/dataaccess.html, accessed on 1 November 2021). Among the 6200 SFs observed, we selected only 289 that presented favorable characteristics for our study. A large part of these flares corresponded with those of published by the service of rapid Magnetic Variation (SRMV) (http://www.obsebre.es/en/rapid, accessed on 1 November 2021).

2.2. Magnetometer Data

The magnetic response to the flares was observed at magnetometer stations distributed over three longitudinal sectors: South and North America, Europe-Africa and Asian-Australia longitudes. The horizontal (H), east (Y) and vertical (Z) components of the geomagnetic field were obtained from the magnetometers belonging to INTERMAGNET (https://www.intermagnet.org/data-donnee/, accessed on 1 November 2021). Figure 1 shows the geographical locations of the magnetic observatories while Table 1 presents their geomagnetic and geographic coordinates. In this study, we selected solar flares which occurred during quiet days provided by the World Data Centre for Geomagnetism, Kyoto, Japan. We computed the magnitude of geomagnetic field (ΔH) using the ΔX and ΔY magnetic components as $\Delta H = (\Delta X^2 + \Delta Y^2)^{1/2}$. In this study, we computed ΔY and ΔZ following the method in [21]. Then, we estimated ΔH using the method proposed in [22]. The amplitude variations in H, Y and Z components before and after the solar flare were estimated.

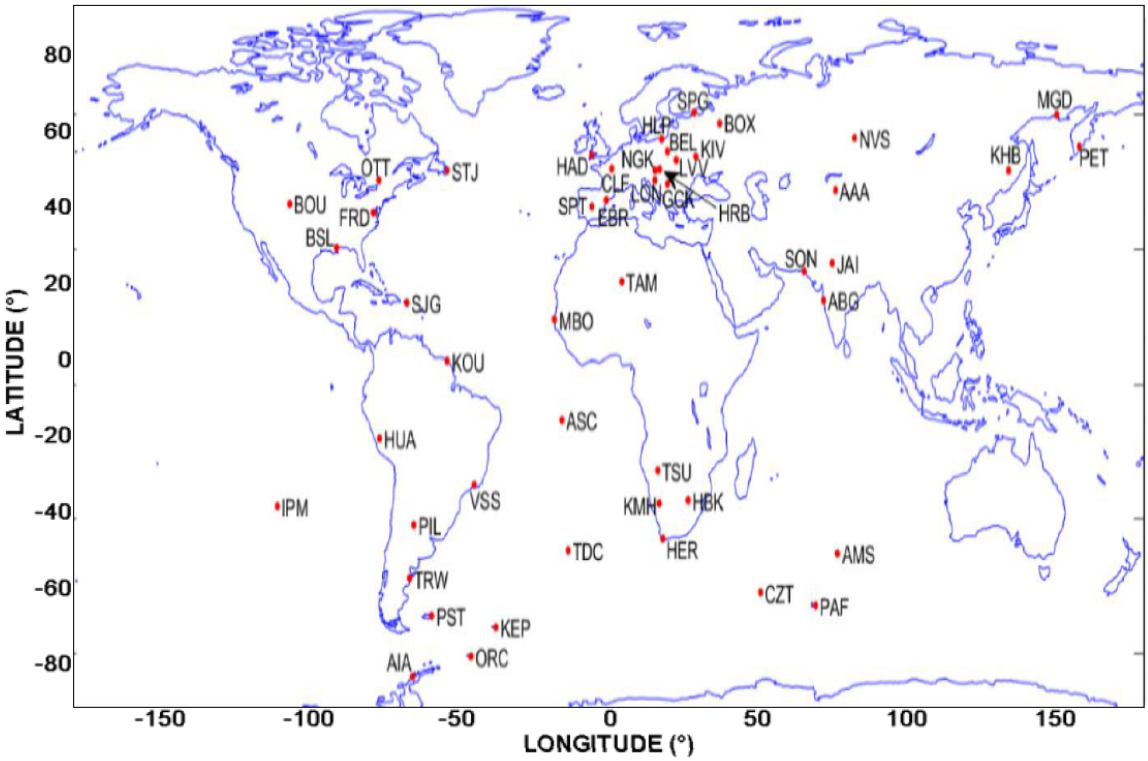

Figure 1. World map with locations of the INTERMAGNET geomagnetic observatories.

Table 1. Geographic and geomagnetic coordinates of magnetic observatories participating in INTERMAGNET.

Observatory	Geographic Latitude (Deg)	Geographic Longitude (Deg)	Geomagnetic Latitude (Deg)	Geomagnetic Longitude (Deg)
AAE	9.02	38.77	5.3	111.8
ABG	18.63	72.87	10.2	146.2
AMS	−37.80	77.57	−46.4	144.3
API	−13.81	188.22	−15.4	262.7
ASP	−23.76	133.88	−32.9	208.2
BNG	4.43	18.56	4.2	91.1
BSL	30.35	−89.64	40.1	339.8
CNB	−35.32	149.36	−42.7	226.9
CTA	−20.08	146.25	28.0	221.0
CZT	−46.44	51.90	−51.4	113.3
DLR	29.50	−100.92	38.3	327.3
EYR	−43.42	172.35	−47.1	253.8
FRD	38.20	−77.37	48.4	353.4
FRN	37.09	−119.72	43.5	305.3
FUR	48.17	11.28	48.4	94.6
GNA	−31.78	115.95	−41.9	188.9
GUA	13.59	144.87	5.3	215.7
GUI	28.32	−16.43	33.8	60.6
HER	−34.43	19.23	−34.0	84
HBK	46.86	18.19	46.9	101.1
HON	21.32	−158.0	21.6	269.7
KDU	−12.69	132.47	−22.0	205.6
KNY	31.42	130.88	21.9	200.8
KOU	5.10	−52.70	11.9	19.5
LER	60.13	−1.18	62.0	89.0
LZH	36.10	103.84	25.9	176.1
MBO	14.38	−16.97	20.1	57.5
MCQ	−54.50	158.95	−60.1	244.3
MMB	43.90	144.20	35.4	211.3
NCK	47.63	16.72	46.9	99.6
NEW	48.27	−117.12	54.9	304.7
NGK	52.07	12.68	51.90	97.6
OTT	45.40	−75.55	55.6	355.3
PAF	−49.35	70.26	−56.9	1382
SJG	18.11	−66.15	28.6	6.1
SPT	39.55	−4.35	42.8	76.0
STJ	47.6	−52;68	57.2	24.0
TAM	22.79	5.52	24.7	81.8
TAN	−18.92	47.55	23.7	115.8
THY	46.9	17.89	46.0	100.5
TUC	32.18	−110.73	39.9	316.0
WING	53.74	129.66	52.6	196.8

The respective amplitude variations X, Y, and Z were computed using Equations (1)–(3).

$$\mathrm{X} = X_1 - X_{00} \tag{1}$$

$$\mathrm{Y} = Y_1 - Y_{00} \tag{2}$$

$$\mathrm{Z} = Z_1 - Z_{00} \tag{3}$$

where X_1, Y_1 and Z_1 are the values of the geomagnetic field components recorded by magnetometers, and X_{00}, Y_{00} and Z_{00} are the mean values of X_1, Y_1 and Z_1 between 23:00 LT to 02:00 LT.

We finally computed the enhancements due to solar flare on the ΔH_{sfe}, ΔY_{sfe} and ΔZ_{sfe} using Equations (4)–(6):

$$\Delta H_{sfe} = \sqrt{(X_{max} - X_{min})^2 + (Y_{max} - Y_{min})^2} \quad (4)$$

$$\Delta Y_{sfe} = Y_{max} - Y_{min} \quad (5)$$

$$\Delta Z_{sfe} = Z_{max} - Z_{min} \quad (6)$$

where H_{max}, Y_{max}, and Z_{max} are the amplitude of geomagnetic components at the peak time of the flare, and X_{min}, Y_{min} and Z_{min} are the values of the field components recorded just before the start time of the flare.

3. Results

3.1. Occurrence Frequency of Solar Flares during Solar Cycles 23 and 24

Figure 2 presents the histograms of the number of solar flares produced per year from 1996 to 2018. The dot line in Figure 2 represents the yearly sunspot numbers profile for the two solar cycles characterized by the different level of solar activity. Solar cycle 23 (SC23) started from to 1996 and ended in 2008 while solar cycle 24 spanned from 2009–2018. Each SF class is represented by a color code. The A, B and C class flares are represented by the blue, green and yellow color, respectively. The M and X classes are represented by the purple and red colors. From 1996 to 2018, there were about 6200 solar flares of all classes, distributed as follows: 37 A-class, 1831 B-class, 3075 C-class, 1113 M-class and 144 X-class flares. We obtained a total of 1025 sunspot numbers in SC23 and 541 in SC24. From SC23 to SC24, we observed a decreasing trend of the sunspot numbers and a corresponding decrease in magnetic activity. This reduction in magnetic activity accounts for the small number of the SFs classes M and X records in SC24.

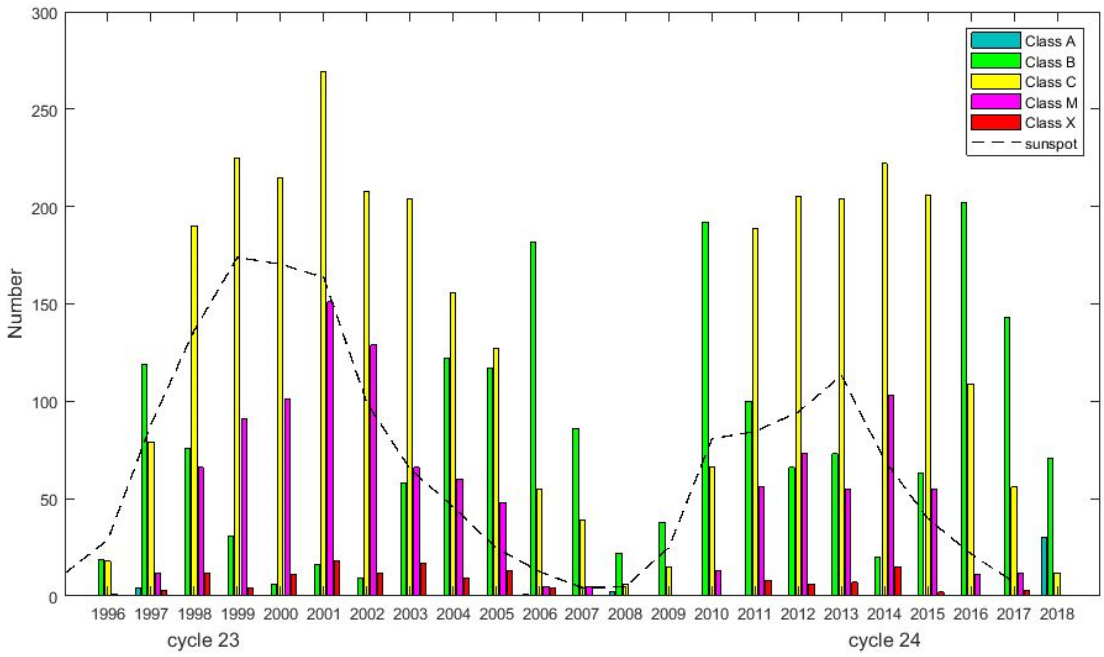

Figure 2. Variation of solar flare occurrence during solar cycles 23 and 24. A-class (blue), B-class (Green), C-class (yellow), M-class (Violet) and X-class (Red). The dotted line represents the sunspots number observed on the sun's surface from 1996 to 2018.

Figure 3 presents the relation between the occurrence of SF of various classes and sunspot number. We took the yearly mean occurrence of flare and sunspot number and computed the correlation coefficient between both quantities. Generally, there was a positive linear relation between solar flare and sunspot number for all flare classes expect A

and B class flares. The correlation coefficients were stronger for C-class (0.93/0.97) and M-class (0.96/0.96) and moderate (0.60/0.56) for X-class during SC23/24, respectively. There was no significant difference in the correlation coefficient between SC23 and SC24 despite the obvious difference in the number of sunspots registered during both solar cycles.

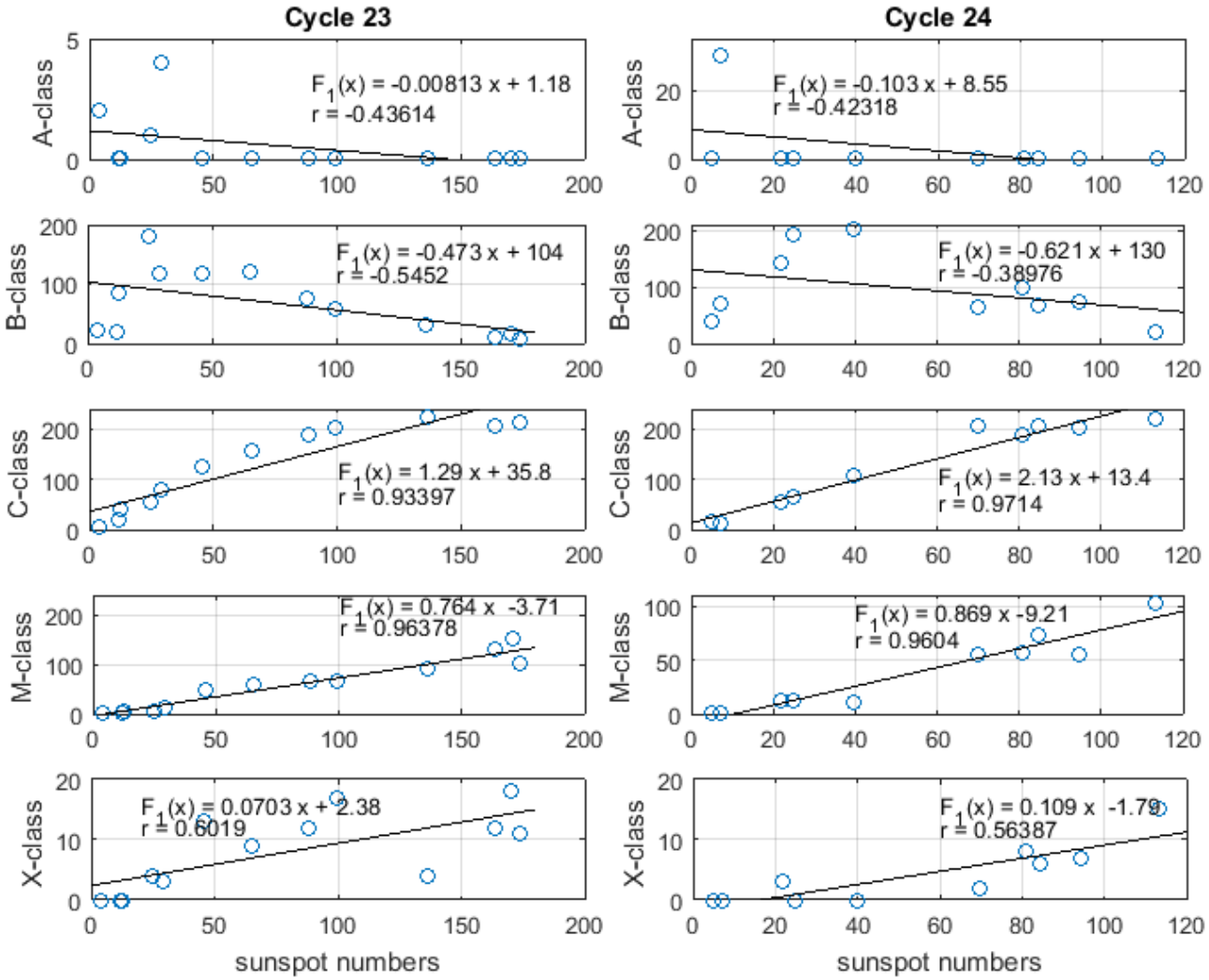

Figure 3. Annual correlation between solar flares and sunspot numbers during cycles 23 and 24.

3.2. Variation of Sfe during Selected Solar Flare Events

We are analyzed a total 289 sfes, 73 sfes associate from X-class and 216 sfes associate from M-class. We noted that from 1996 to 2000, the AR of about 23 flares whose effects could still be felt on the geomagnetic field components, had no information about their location on the solar disc. Oppositely, from 2001 to 2018, the AR of 266 flares, had information about their location. Therefore, it was found that 61 of them occurred at the center of the solar disc, 150 on the limb and 55 between the center and the limb otherwise referred to as the "Intermediate Zone" in this work. Table 2 presents the distribution of the flare according to their location on the solar disc.

Table 2. Results of solar flare identified on the sun surface.

Flare Class	Number	Center	Intermediate Zone	Limb
X	73	17	12	44
M	193	44	43	106
Total	266	61	55	150

Based on the flare location on the solar disc, we have distinguished relevant categories of sfe on the geomagnetic field components. An example of each flare class has been analyzed as case study. These include the X2.6 solar flare of 27 November 1997, X9.4 solar flare of 06 November 1997, M1.4 and M4.2 solar flares of 03 November 1997, X1.5 solar flare of 03 July 2002, X6.4 solar flare of 13 December 2001, and X1.7 and X2.1 solar flares of 25 October 2013.

3.2.1. The X2.6 Solar Flare of 27 November 1997

On 27 November 1997, an X2.6 solar flare occurred from the active region (AR) 8113 on the sun's surface. GOES satellites located this AR at the geographic coordinates N20E77. Figure 4 (on top) shows the X-ray flux in the wavelength band 0.1–0.8 Â. This solar flare lasted for about 21 min as it began by 12:59 UT and ended at 13:20 UT. It reached its peak at approximately 13:17 UT.

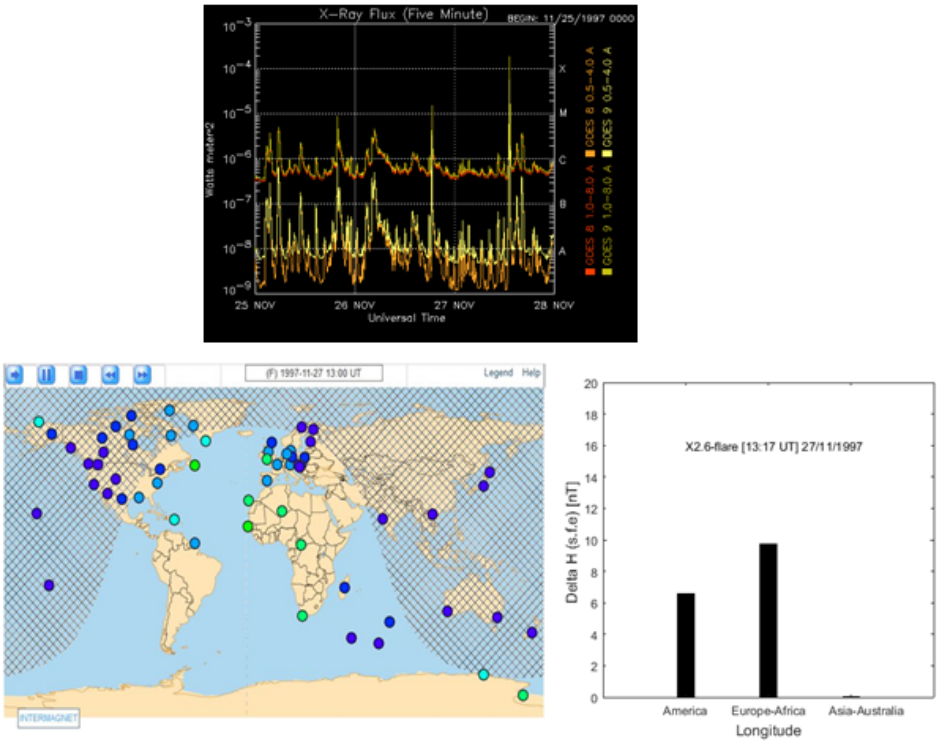

(**a**) (**b**)

Figure 4. X-ray flux of X2.6 solar flare of 27 November 1997 (www.speaceweather.com/archive.php, accessed on 1 November 2021). The illuminated part of the Earth during this solar flare of 27 November 1997, is shown in Figure 4, with noon in UT closer to Europe-Africa longitude sector (on **top**) and **below**. Day and night alternation Source INTERMAGNET (**a**) and histograms of the average variations of magnetic crochets in South and North America, Europe-Africa and Asia-Australia longitude sectors from 11 November 1997 at 13:17 UT (**b**).

The illuminated part of the Earth during this flare of 27 November 1997, is shown in Figure 4 (left below), with noon in UT closer to Europe-Africa longitude sector. Table 3 presents data obtained from the magnetic stations located on the illuminated part of the Earth during this event. This table contains the IAGA codes of observatories, the solar zenith angle (SZA) calculated from the website http://www.solartopo.com/orbite-solaire.htm, accessed on 1 November 2021, the magnetic crochet value and the universal time of occurrence of the maximum sfe at each station. From this Table 3, it can be seen that the strongest magnetic responses associated with the X2.6 was observed mainly at stations with a low solar zenith angle and which were close to the magnetic equator during the

local noon. This was the case of GUI, TAM, STJ, HER and MBO. We also noted that the sfe was not observed simultaneously at all observatories. The time interval varied by few seconds from one station to another. It was observed from Figure 4 (right-below) dealing with the sfe in the South and North America, Europe-Africa and Asia-Australia longitudes during the X2.6 flare event of 27 November 1997, the mean magnetic amplitude of sfe was stronger in the Europe-Africa sector.

Table 3. The magnetic response to the X2.6 solar flare of 27 November 1997.

Observatory	Solar Zenith Angle (Deg)	ΔH_{Sfe} (nT)	Time (UT)	ΔY_{Sfe} (nT)	ΔZ_{Sfe} (nT)
BNG	28.40	9.64	13:18	−6.3	0.6
BSL	52.23	6.11	13:19	−5.01	0.2
CZT	27.92	5.63	13:19	−5.3	3.2
FRD	59.77	8.45	13:19	−7.48	2.8
GUI	50.37	19.65	13:19	6.61	−5.8
HER	13.95	19.83	13:19	−18.48	−6.9
KOU	26.61	6.26	13:18	−4.9	7.9
LER	81.45	4.90	13:19	5.16	−3.2
MBO	36.99	24.21	13:19	13.5	−7.1
OTT	66.96	10.30	13:18	−8.5	0.3
PAF	28.43	3.55	13:18	−2.2	1.8
SJG	39.85	8.25	13:18	−6.13	−3.8
SPT	63.39	11.27	13:18	−10	1.1
STJ	69.11	17.96	13:19	−12.6	24.2
TAM	45.35	24.12	13:19	13.3	−1
TAN	9.59	5.96	13:21	−7	2.4
THY	68.75	NAN	NAN	NAN	NAN
WING	74.81	14.14	13:18	10	0.2

The latitudinal variation of the magnetic response to the X2.6 solar flare is shown in Figure 5. This figure deals with the diurnal variation of the horizontal (H), eastward (Y) and vertical (Z) components of the Earth's geomagnetic field on 27 November 1997, at stations located in the Europe-Africa longitude. At the MBO station, H suddenly increased and reached a maximum at approximately 13:19 LT. It then dropped and returned to its normal variation at approximately 13:23 LT. The sudden increase in H was observed simultaneously at all stations, but its amplitude differed from one station to the other. For example, it decreased from the stations located close to the magnetic equator to those at the boundaries of the northern and southern hemispheres. The magnetic signature of the flare (ΔH_{sfe}) otherwise known as the magnetic crochet was positive at low latitudes and negative at mid-latitudes. For the X2.6 solar flare, the maximum value of the magnetic crochet was recorded at MBO (ΔH_{sfe} = 24.21 nT) rather than BNG (ΔH_{sfe} = 9.64 nT) which is closer to the magnetic equator. The corresponding local time of occurrence of the peak solar flare effect was 14:01 LT at the BNG station. For the Eastward component (Y), the magnetic response associated with the November 27, 1997, flare manifested in the form of a negative crochet in the Northern Hemisphere and positive crochet in the Southern Hemisphere. The amplitude reversal occurred between the equatorial stations MBO and BNG. The maximum values of sfe were observed at MBO, were ΔY_{sfe} = 13.5 nT at 13:19 LT and ΔY_{sfe} = −6.3 nT at BNG.

The magnetic crochet for the vertical component (Z) had strong amplitudes around the magnetic equator. The maximum value was also observed at MBO, with ΔZ_{sfe} = −7.1 nT at 13:19 LT. We also noticed a reversal of the signs in the amplitude of the magnetic crochet between the GUI, MBO and BNG stations. This value is ΔZ_{sfe} = −0.6 nT at BNG.

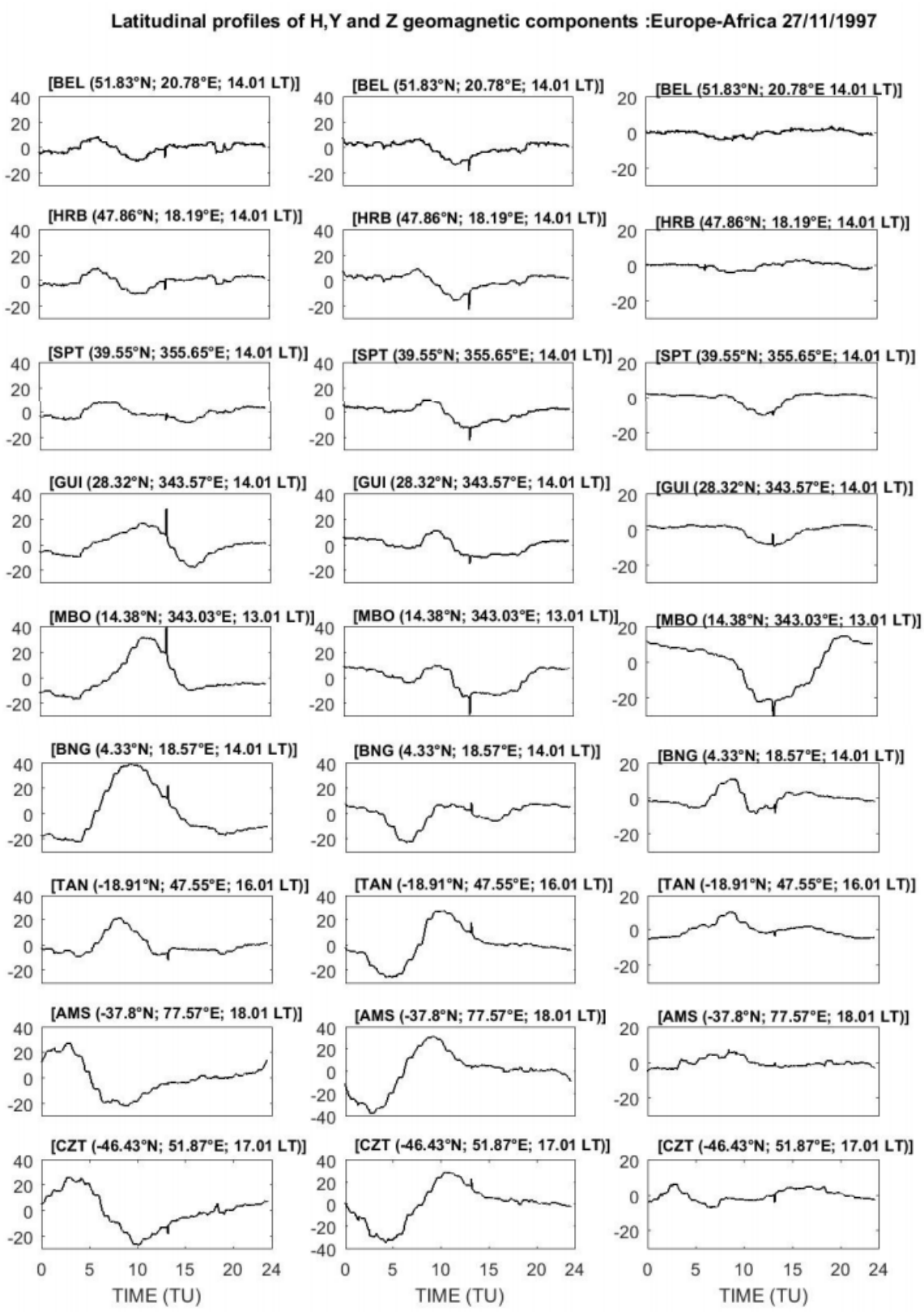

Figure 5. Latitude variation of horizontal (H), eastward (Y), and vertical (Z) components of the geomagnetic field during the X2.6 solar flare of 27 November 1997.

3.2.2. The X9.4 Solar Flare of 6 November 1997

Figure 6a shows the variation of the X-ray flux during the X9.4 solar flare of 6 November 1997. This flare originated from AR 8100 which was located at S21W53. It began at 11:49

UT, reached its peak at 11:55 UT and ended at 12:09 UT. The flare, therefore, lasted for approximately 20 min. The magnetic response associated with this flare is presented in Table 4. The peak amplitudes of the crochets at the magnetometer stations during the solar flare X9.4 are shown in Table 4. This solar flare had a greater magnetic effect at the respective stations. From Figure 6b, the Europe-Africa longitude registered the highest amplitude of the mean magnetic crochet. We therefore limited the analysis of the sfe associated related to this flare to this longitude. In line with this, variations of the geomagnetic components are presented in Figure 7. Despite the strong variation of the geomagnetic components on this day, the magnetic signature of the X9.4 solar flare could still be clearly distinguished at about 12:00 LT. The magnetic crochets were negative at mid-latitudes and positive around the magnetic equator. The fluctuations in the H, Y and Z components from 15:00 UT could have been due to the weak increase in polar cap potential as Dst decreased slightly to reach a minimum of −34 nT at 17:30 UT (not shown). Stations located close to the magnetic equator recorded the highest values of the amplitude of the crochet at about 11:55 LT with MBO recorded a peak ΔH_{sfe} of 56.44 nT at 12:00 LT.

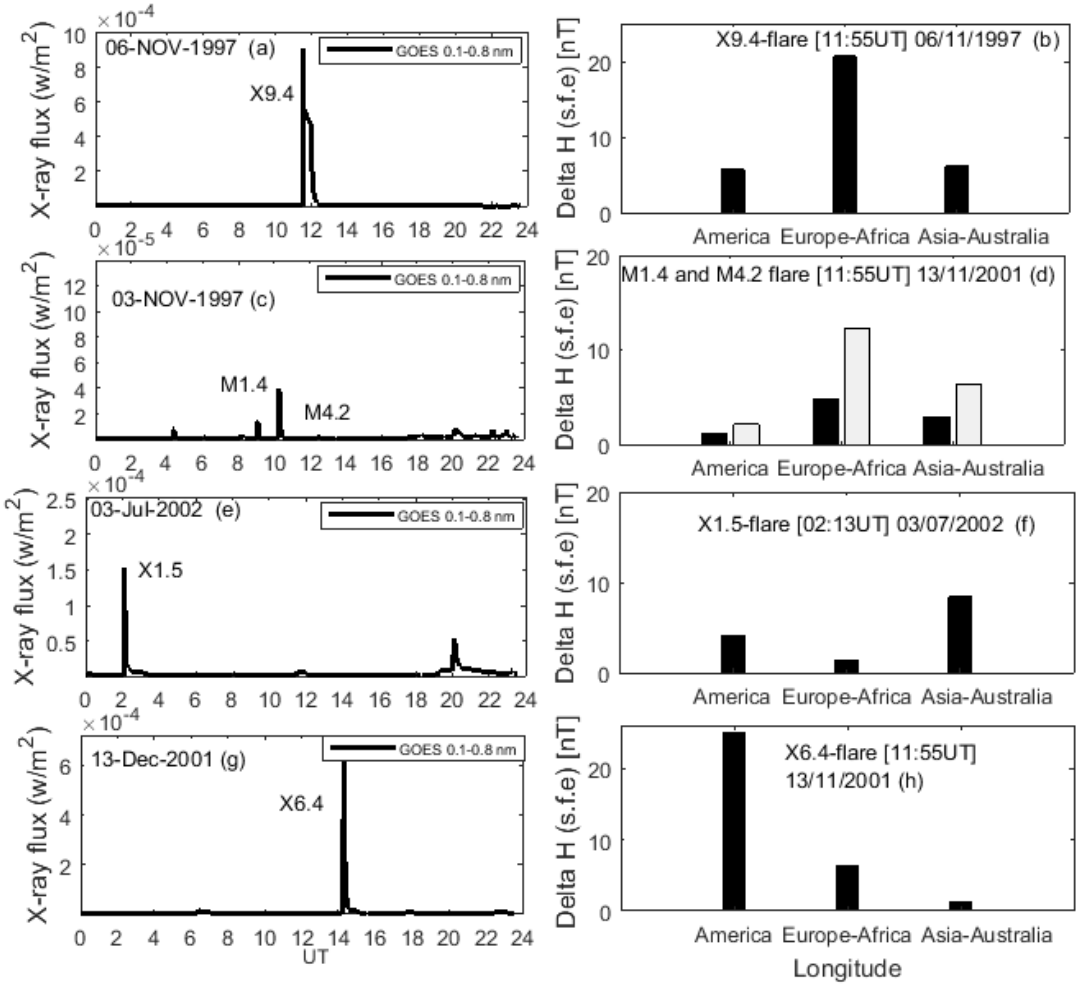

Figure 6. X-ray flux and histograms of the average variations of magnetic crochets in South and North America, Europe-Africa and Asia-Australia longitude sectors for X9.4 solar flare of 6 November 1997, M1.4 and M4.2 solar flares of 3 November 1997, X1.5 solar flare of 3 July 2002, X6.4 solar flare of 13 December 2001, and X1.7 and X2.1 solar flares of 25 October 2013. (**a**,**b**) show respectively X-ray flux and mean variation of Hsfe for X9.4, (**c**,**d**) show respectively X-ray flux and mean Hsfe for M1.4 and M4.2, (**e**,**f**) show respectively X-ray flux and mean Hsfe for X1.5, then (**g**,**h**) show respectively X-ray flux and mean Hsfe for X6.4.

Table 4. The magnetic response to the solar flare X9.4 of 06/11/1997.

Observatory	Solar Zenith Angle (Deg)	ΔH_{sfe} (nT)	Time (UT)	ΔY_{Sfe} (nT)	ΔZ_{Sfe} (nT)
ABG	40.76	7.47	11:59	3.28	2.9
BNG	23.04	55.22	11:58	−46.5	−16.3
CZT	30.80	0.8	11:52	−0.4	3.7
FUR	65.79	3	11:52	3	0
GUI	52.31	34.34	12:00	−7.61	0.4
HER	27.62	1.38	11:55	−1.38	−10.4
KOU	28.97	7.18	12:00	7.3	−1.6
MBO	41.94	56.44	12:00	19.1	26.5
NCK	64.35	2.08	11:52	1.8	−0.5
NGK	69.27	4	11:52	3.84	−0.6
PAF	36.13	1.61	11:52	0.8	−0.1
SJG	39.04	0.88	11:52	−0.69	0.1
SPT	63.27	2.88	11:52	2.26	0.2
STJ	64.64	14.63	11:59	−7.6	1.6
TAM	45.76	41.98	11:57	10.3	5.2
TAN	9.77	23.62	11:56	−9.1	8
WING	71.46	3.16	11:52	3	0

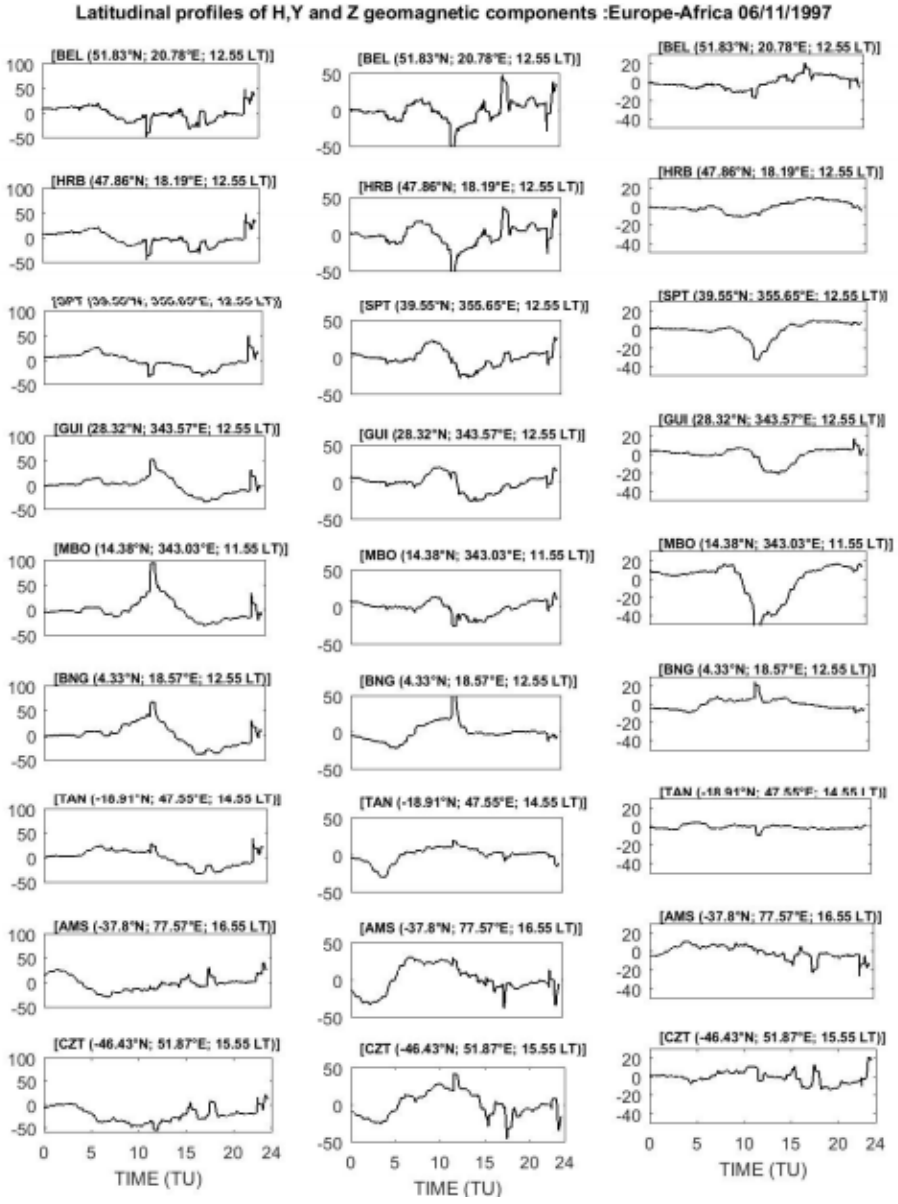

Figure 7. Variation of the horizontal (H), eastward (Y) and vertical (Z) components of the geomagnetic field during the X9.4 solar flare on 6 November 1997.

The eastward component (Y) also exhibited the negative magnetic crochet at all stations except in CZT. The magnitudes of the crochet on the Y component were generally strong near the magnetic equator. The sfe maximum value was observed in BNG with $\Delta Y_{sfe} = -46.73$ nT at 11:58 LT. Furthermore, the vertical component (Z) showed the negative magnetic crochet in all stations except in the BNG station, where the maximum peak was $\Delta Z_{sfe} = -16.30$ nT.

3.2.3. The M1.4 and M4.2 Solar Flares of 3 November 1997

We equally investigated an interesting case when the same AR successive flares were produced from the same AR. This was the case of the M1.4 and M4.2 class flares of 3 November 1997. The X-ray flux during these flares which originated from AR 8100 is shown in Figure 6c. The M1.4-class flare occurred from 09:03 UT to 09:13 UT (~10 min) while the second M4.2 started at 10:18 UT and ended at 10:34 UT (~16 min). The geographical positions of the AR responsible of these flares were S20W30 and S19W12 for the M1.4-class and M4.2-class, respectively. The sfe on the H component flares is presented in Table 5.

Table 5. The magnetic observatories data of solar flare M1.4 and M4.2 of 3 November 1997.

Observatory	Solar Zenithal Angle (Deg)	ΔH_{Sfe} (nT) for M1.4	Time (UT)	Solar Zenithal Angle (Deg)	ΔH_{Sfe} (nT) for M4.2	Time (UT)
ABG	70.9	1.42	9:09	54.25	5.83	10:32
AMS	58.42	7.1	9:10	46.62	10.31	10:30
BNG	53.06	7.54	9:13	35.62	14.32	10:31
FUR	81.01	1	9:12	71.48	5.09	10:31
GNA	54.73	0.3	9:11	38.23	5.83	10:31
GUI	80.15	2.55	9:13	65.02	5.78	10:33
HER	60.35	3.59	9:11	44.25	0.77	10:31
MBO	75.50	2.4	09:10	58.08	12.4	10:34
NCK	77.77	4.23	9:09	68.88	5.04	10:33
NGK	82.51	3.5	9:09	74.01	11.66	10:30
PAF	58.06	7.1	9:09	46.35	13.12	10:29
SPT	85.13	3.9	9:11	72.81	4.68	10:32
TAN	48.62	12.79	9:10	29.05	21.21	10:29
THY	76.72	3.53	9:10	67.86	6.53	10:29
WING	85.82	2.82	9:13	76.63	10	10;29

Observatories around the magnetic equator with a low SZA had the highest magnetic peaks. The sfe was pronounced in the Europe-Africa sector as seen in Figure 6d. Also, from Figure 8 showing the variation of the sfe with latitude during the M1.4 and M4.2 flares, the magnetic crochets had similar variations on the H, Y and Z components. In addition, the variations in the peak H were not different from the previous cases examined. The peak magnetic crochets associated with the M1.4 class flare amplitude was smaller than the one associated with the M4.2 class flare. The maximum values of sfe recorded at TAN were $\Delta H_{sfe} = 21.21$ nT for class M4.2 solar flare at 10:31 LT and $\Delta H_{sfe} = 12.79$ nT for class M1.4 solar flare at 09:13 LT.

The Y component exhibited a positive peak at all magnetic station. This characteristic was different from what we have observed so far. Furthermore, the magnetic crochets associated with the flare class M4.2 were stronger than those of the class M1.4 with $\Delta Y_{sfe} = 31.80$ nT for class M1.4 flare at 9:10 LT and $\Delta Y_{sfe} = 30.10$ nT for the class M4.2 flare at 10:31 LT at the AMS station.

On the Z component, the magnetic crochets associated with M4.2 were stronger than those of the M1.2 solar flare. The maximum sfe values at the BNG station were: $\Delta Z_{sfe} = 19.82$ nT at 10:31 LT for the class M4.2 flare and $\Delta Z_{sfe} = 16.62$ nT at 09:11 LT for class M1.4 flare.

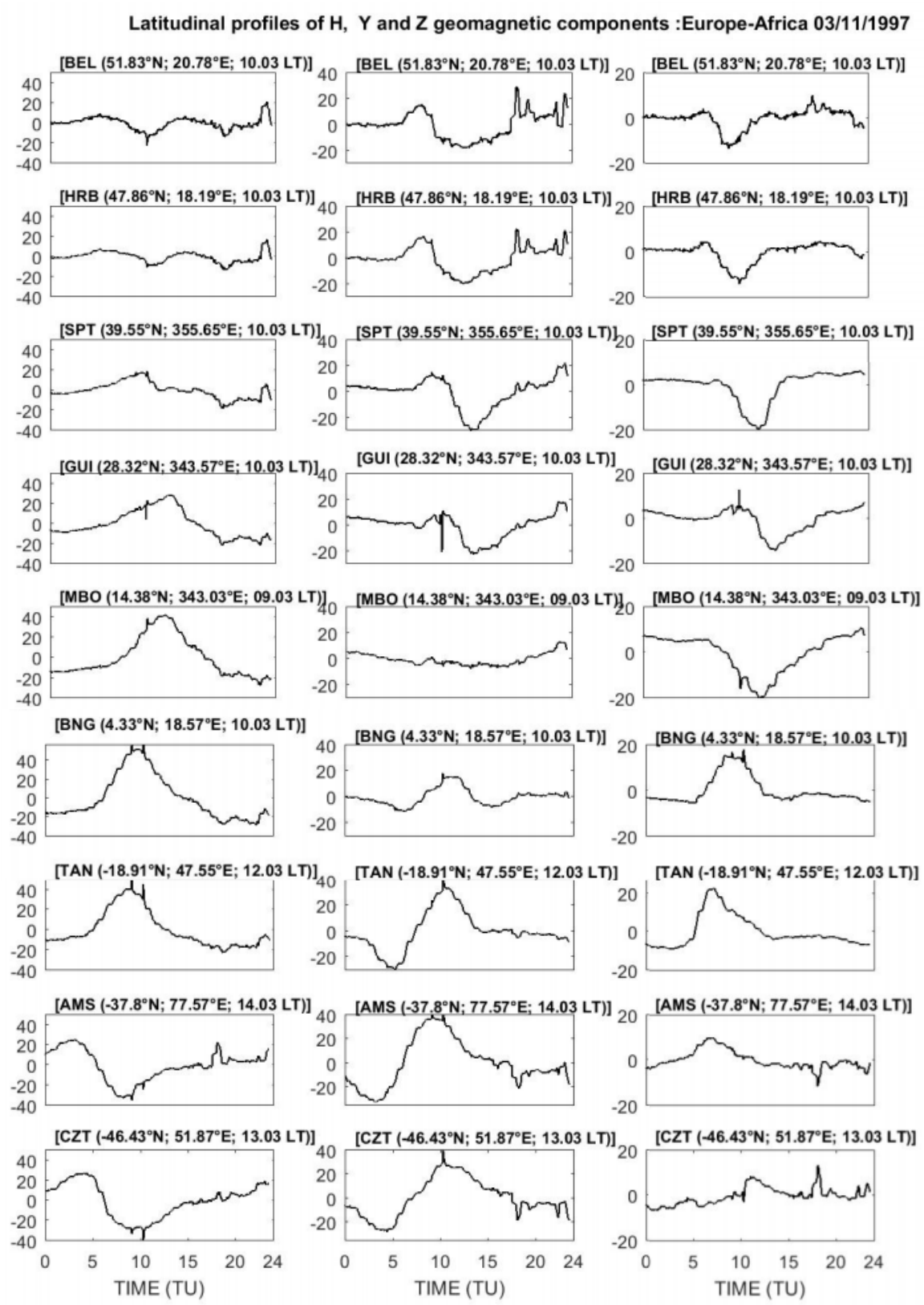

Figure 8. Variation of horizontal (H), eastward (Y) and vertical (Z) components of the geomagnetic field during the M1.4 and M4.2 solar flares of 3 November 1997.

3.2.4. The X1.5 Solar Flare of 3 July 2002

Figure 6e shows the X-ray flux during the X1.5 solar flare that occurred on 3 July 2002 on AR 0017. This flare started at 02:08 UT, peaked at 02:13 UT and ended at 02:16 UT. It therefore lasted ~5 min. The geographic position of the sunspot from which this flare emanated was S18W51. Table 6 presents the characteristics of stations located at the mid and low-latitudes as well as their corresponding sfes on 3 July 2002 at 02:08 UT. From this table, most magnetic stations with high crochet were characterized by low SZA and were close to the magnetic equator during the local noon. These stations were located in the Asia-Australia longitude. The time of occurrence of the peak crocket in the different stations differed from one place to another with a time difference of just few seconds. Figure 6f shows the mean distribution of sfe in the different longitude sectors. The magnetic crochet over the Europe-Africa longitude was almost zero at 02:13 UT on 3 July 2002 given that stations over this sector were still in the early morning period. The Asia-Australia longitude sector on the other hand, recorded the highest crochet value. The magnetic crochet of the H component in this sector was stronger than in the American sector.

Table 6. The magnetic response to the solar flare X1.5 of 3 July 2002.

Observatory	Solar Zenith Angle (Deg)	ΔH_{Sfe} (nT)	Time (UT)	ΔY_{Sfe} (nT)	ΔZ_{Sfe} (nT)
ABG	42.48	16.41	02:15	15.61	11.2
API	25.79	4.32	02:13	−4.18	1.7
ASP	12.63	14.04	02:15	7.3	−4.8
CNB	18.89	10.01	02:15	−5.6	−1.7
CTA	12.63	17.61	02:13	0.8	1.3
EYR	24.07	6.04	02:15	−0.78	1.1
FRN	67.17	8.96	02:15	−6.22	−0.8
GNA	29.43	3.84	02:14	3.4	−0.2
GUA	38.46	15.96	02:13	6.91	2.9
HON	50.32	4.26	02:17	−2.66	−1.2
KDU	12.54	13.8	02:15	−0.5	−0.5
KNY	55.93	0.1	02:13	−0.01	1.8
LZH	59.19	5.53	02:13	−1.6	0.8
MCQ	37.79	6.67	02:15	1	−2.9
MMB	71.25	2.95	02:13	9.61	−1
NEW	67.39	9.12	02:13	−7.05	0.2
TUC	60.7	5.9	02:15	−3.53	1.2

The perturbation on the geomagnetic components associated with the X1.5-class solar flare of 3 July 2002 is shown in Figure 9. The H component had similar variation to the one observed on 27 November 1997. However, the inversions of the amplitudes of the magnetic crochets occurred between the low latitude and mid-latitude.

The maximum amplitude was observed at about 12:15 LT at the CTA station, with ΔH_{sfe} = 17.61 nT. The eastward (Y) component also exhibited similar variations to those in the previous case. The magnetic crochet reversed over the magnetic equator. It was positive in the Northern hemisphere and negative in the Southern hemisphere. The highest value of sfe was recorded at 07:15 LT in the ABG station (ΔY_{sfe} = 15.61 nT). For the Z component, the sfe was negative at all stations located in the Northern hemisphere, in contrast to those in the equatorial region and the Southern hemisphere where the magnetic crochets were either positive or negative. The maximum value of the sfe on the Z component was recorded at ABG station, with value of ΔZ_{sfe} = 11.2 nT at 07:15 LT.

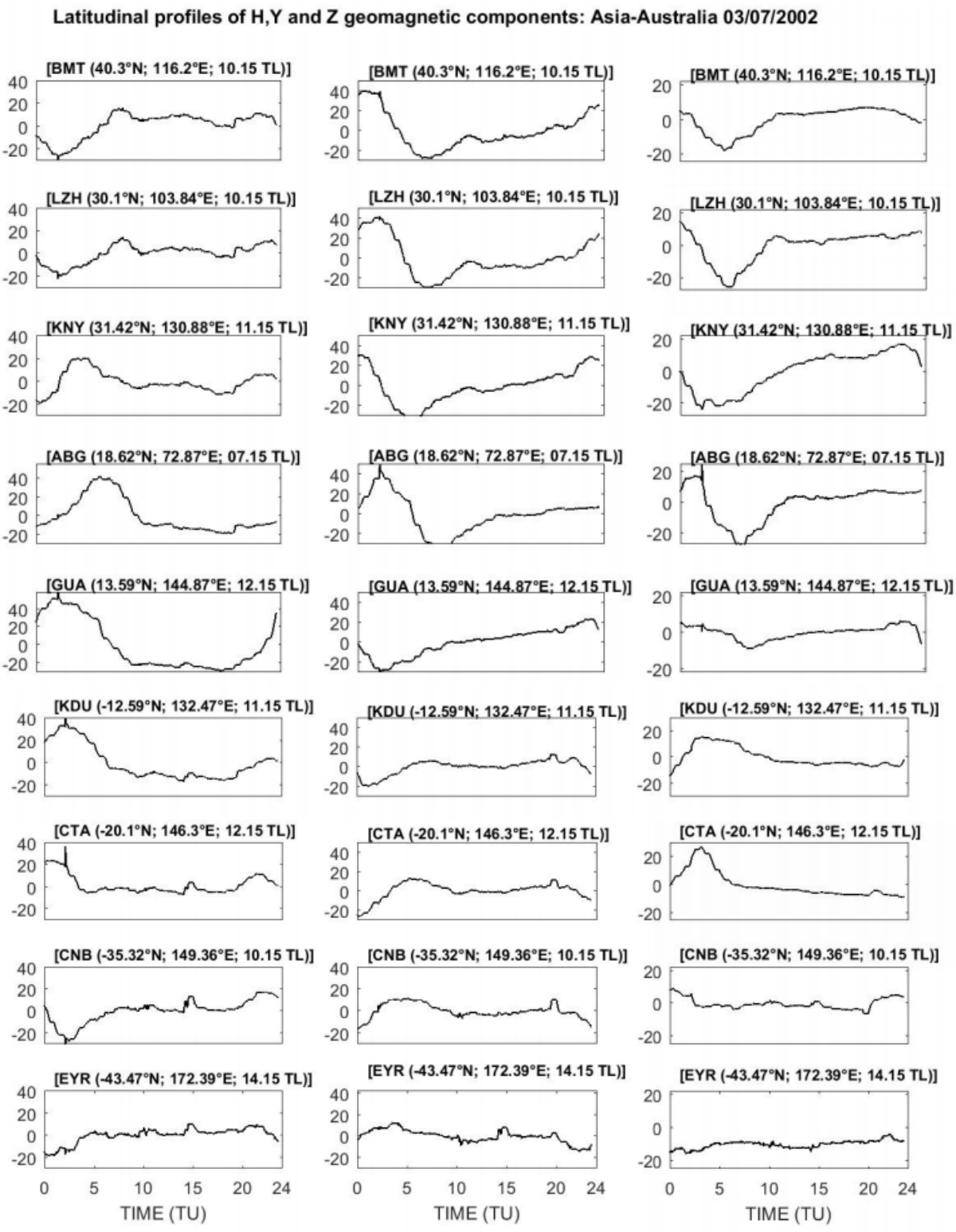

Figure 9. Variation of horizontal (H), eastward (Y) and vertical (Z) components of the geomagnetic field during the X1.5 solar flare of 3 July 2002.

3.2.5. The X6.4 Solar Flare of 13 December 2001

The X6.4 flare of 13 December 2001 originated from the active region 9733 which was located at N14E18. During this event, the sfe was observed simultaneously over stations in the American and Africa-European longitudes. Figure 6g presents the variations of the solar flux during this event. The flare started at 14:20 UT and reached its maximum at

14:30 UT, and ended at 14:35 UT. Thus, it lasted for ~15 min. All stations that the flare effect was detected during this event are shown in the Table 7. Despite a high SZA certain stations in America recorded sometimes a high peak of sfe than those in the Africa-Europe sector. The histograms in Figure 6e confirm that the sfe was pronounced in the American longitude during this event.

Table 7. The magnetic observatories data of solar flare X6.4 of 13 December 2001.

Observatory	Solar Zenithal Angle (Deg)	ΔH_{Sfe} (nT)	Time (UT)	ΔY_{Sfe} (nT)	ΔZ_{Sfe} (nT)
AAE	36.52	4.03	14:32	3.5	−1.3
BNG	36.7	17.21	14:30	15.4	−3.1
BSL	65.52	24.85	14:31	20.87	−3.5
CZT	33.96	6.35	14:32	15.11	2.7
DLR	59.03	19.92	14:31	6.3	0.5
FRD	70.3	28.83	14:31	19.33	8.4
FUR	77.94	8.57	14:31	7.3	−4
GUI	51.98	19	14:32	−21.27	8
HBK	20.18	20.7	14:30	−21.7	3.1
HER	16.09	10.45	14:39	−10.4	−1.4
KOU	41.65	17.2	14:30	−3.5	−19.5
MBO	38.19	10.46	14:26	−29.3	−14.2
NCK	79.56	4.81	14:29	4.38	−2.62
NGK	81.67	5.68	14:31	4.7	−4.5
OTT	76.85	32.02	14:30	24.7	−9.7
PAF	80.44	2.35	14:28	0.5	0.3
SJG	52.52	13.74	14:31	−13.74	−6.9
SPT	68.22	18.79	14:31	−17.56	4.5
STJ	78.76	32.64	14:31	−2	−14.7
TAM	48.86	10.78	14:31	3.2	2
TAN	25.03	2.59	14:29	−2.3	0.8
THY	79.51	2.59	14:31	5.2	−3
VSS	36.99	66.65	14:31	4.52	20.1
WING	81.9	6.08	14:31	4.1	−1

Figure 10a,b shows the sfe on the geomagnetic H, Y and Z components recorded in the South America and Europe-Africa longitudes. The magnetic equator in the South America sector was located around the SJG and KOU, while it was located between MBO and BNG for the African longitude. The sfe on the H component was always reversed between the mid and low-latitudes in both sectors, with a difference in the magnitude of the magnetic crochets. The amplitudes of the Magnetic crochets were greater in the America than Europe-Africa sector. At VSS, the peak ΔH_{sfe} was 66.65 nT at 11:20 LT in the American sector and 14.01 nT at 14:20 LT in MBO for the Europe-African sector.

Furthermore, the amplitude of the magnetic crochets on the Eastward component (Y) was positive in most stations except at KOU where it was negative. The maximum value of sfe recorded at OTT was ΔY_{sfe} = 24.7 nT at 11:20 LT. From Figure 10b, the amplitude of the magnetic crochets was negative from BEL to MBO and positive from BNG to CZT stations. The maximum value of the magnetic crochet on the Eastward Y component occurred at MBO ($|\Delta Ysfe|$ = 29.3 nT to 14:26 LT). Moreover, it was noted that for the same flare the magnetic effect of the Y component differed in the two longitudes under consideration.

Variation of the magnetic crochet on Z was inconsistent and different in both longitudes. The inversion of the crochet occurred in both hemispheres, and around the magnetic dip equator. For this component, the maximum value of the solar flare effects was observed at the VSS station, with a value of ΔZ_{sfe} = 20.1 nT at 11:20 LT in the American sector, and at MBO with $|\Delta Z_{sfe}|$ = 14.2 nT à 14:20 LT in the Europe-Africa sector.

(**a**)

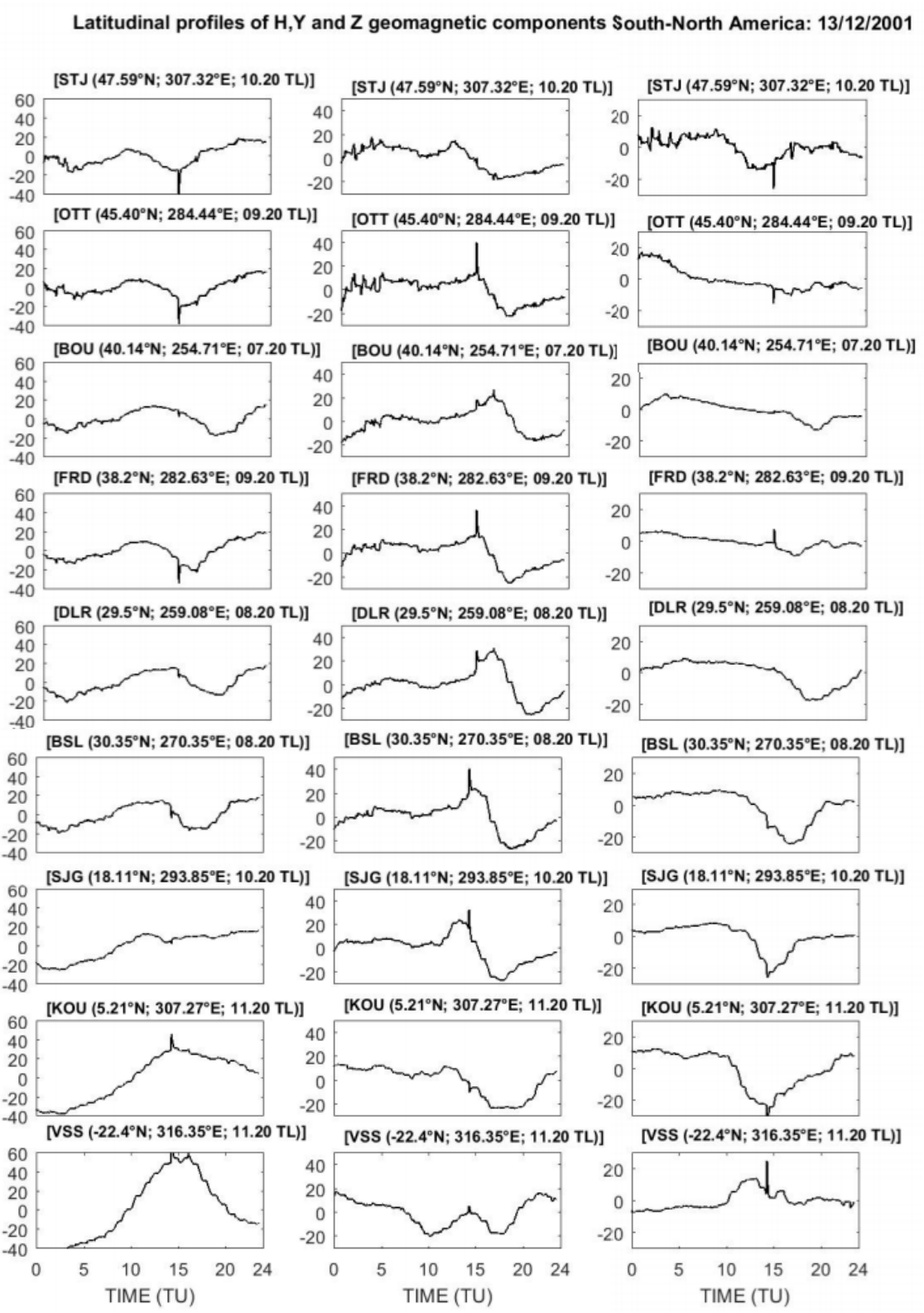

Figure 10. *Cont*.

(**b**)

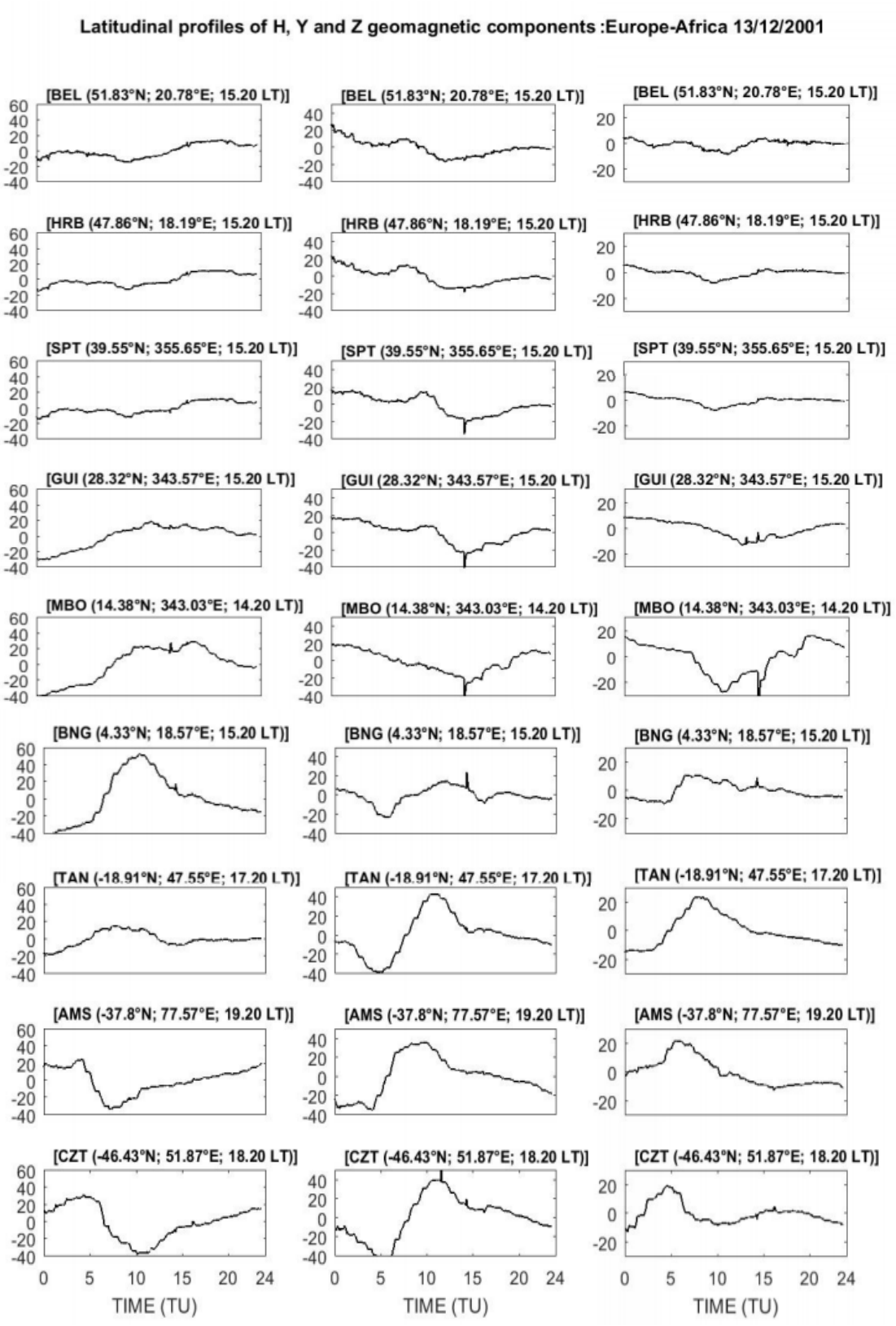

Figure 10. (**a**) Variation of horizontal H, easterly Y and vertical Z components of the geomagnetic field associated with the solar eruption class X6.2 on 13 December 2001 (American longitude sector) (**b**) Variation of horizontal H, easterly Y and vertical Z components of the geomagnetic field associated with the solar eruption class X6.2 on 13 December 2001 (Africa longitude sector).

3.2.6. The X1.7 and X2.1 Solar Flares of 25 October 2013

In Figure 11, we presented two examples of solar flares which occurred successively in the same AR 1882 on 25 October 2013. The X1.7 class flare started at 07:53 LT, reached its peak at 08:01 LT and ended at 08:09 LT, while the X2.1 one that started at 14:51 LT reached its peak at 15:03 LT and ended at 15:12 LT (Figure 11a). The effect of both flares was observed in the Europe-Africa longitude. Their magnetic effects on the H component are shown in Figure 11b. It was observed that irrespective of the flare class, the sfe on H was pronounced when the flare occurred around the local noon at a particular station. For example, the X1.7 resulted in a greater magnetic crochet on H in AAE which was in the local noon. The AAE and SPT stations, recorded the respective peak sfe values of 40.60 nT and 6.53 nT for Class X1.7 flare, and 0.70 nT and 5.2 nT for Class X2.1 flare. For the ASC, DBV and GUI stations, the magnetic effects of the X2.1 class solar flare on H were stronger than those of Class X1.7. The summary synthesis of all class study is presented in the Table 8.

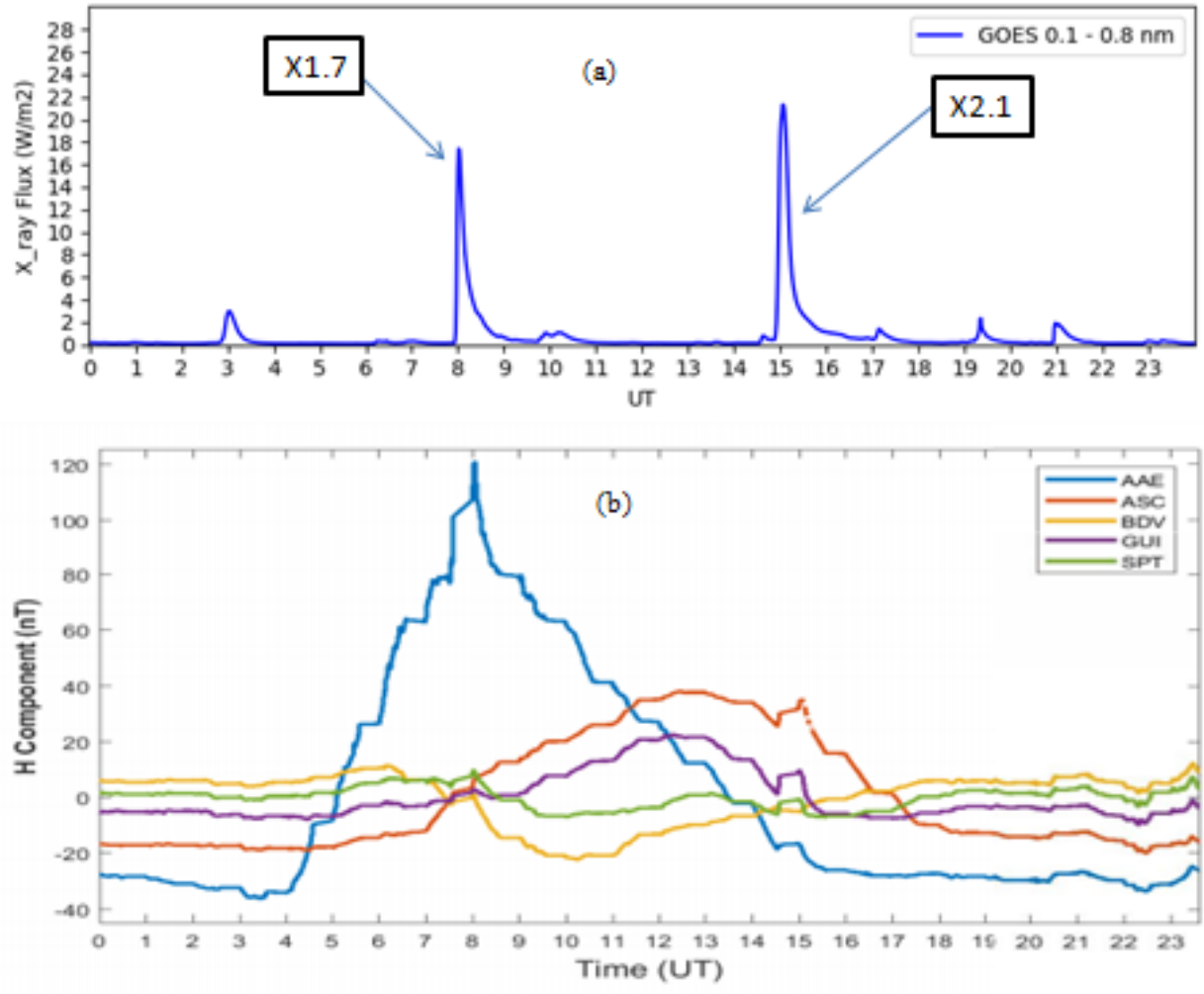

Figure 11. (**a**) Magnetic effects of the X1.7 and X2.1 solar flares of 25 October 2013, and (**b**) on the H component at different observatories.

Table 8. Summary synthesis of all class study.

Class	Characteristics of the Class Location on the Sun Electromagnetic Emission Time Duration	Example	Time and Maximum Peak of Sfe
Class 1	Active region: 8113 Position: N20E77 (limb) X rays fluxes: 0.1–0.8 Â Time: 12:59 UT to 13:20 UT. Peak at 13:17 UT	X2.6 solar flare of 27 November 1997	Time: 13:19 UT ΔH_{Sfe}= 24.21 nT
Class 2	Active region: 8100 Position: S21W53 (limb) X rays fluxes: 0.1–0.8 Â Time: 11:49 UT to 12:09 UT. Peak at 11:55 UT	X9.4 solar flare of 6 November 1997	Time: 12:00 UT ΔH_{Sfe} = 56.44 nT
Class 3	Active region: 8100 Position: S20W30 for M1.4 and S19W12 for M4.2 (center) X rays fluxes: 0.1–0.8 Â Time: 09:03 UT to 09:13 UT. Peak at 09:10 UT for M1.4 Time: 10:18 UT to 10:34 UT. Peak at 10:29 UT for M1.4	M1.4 and M4.2 solar flares of 3 November 1997	Time: 9:13 UT ΔH_{Sfe} = 12.79 nT for M1.4 Time: 10:31 UT ΔH_{Sfe} =21.21 nT for M4.2
Class 4	Active region: 0017 Position: S18W51 (transition zone) X rays fluxes: 0.1–0.8 Â Time: 02:08 UT to 02:16 UT. Peak at 02:13 UT	X1.5 solar flare of 3 July 2002	Time: 02:13 UT ΔH_{Sfe} =17.61 nT
Class 6	Active region: 9733 Position: N14E18 (center) X rays fluxes: 0.1–0.8 Â Time: 14:20 UT to 14:30 UT. Peak at 14:35 UT	X6.4 solar flare of 13 December 2001	Time: 14:31 UT ΔH_{Sfe} = 66.65 nT
Class 7	Active region: 1882 Position: S08E73 (limb) X rays fluxes: 0.1–0.8 Â Time: 07:53 UT to 08:09 UT. Peak at 08:01 UT for X1.7 Time: 14:51 UT to 15:12 UT. Peak at 15:03 UT for X2.1	X1.7 and X2.1 solar flares of 25 October 2013.	Time:08:04 UT X1.7 ΔH_{Sfe} = 42.62 nT in AAE station Time:08:04 UT X2.1 ΔH_{Sfe} =8.31 nT in ASC station

3.3. Monthly/Seasonal Variation of the Sfe for Cycles 23 and 24

Figure 12 shows the monthly variation of sfe observed during cycles 23 and 24. The dot (bold) lines represent the monthly average values derived during solar cycle 23 (cycle 24). The error bars are the standard deviations, and the solid curves are the average variations of the sfe. The long error bars indicate that these measurements have a large variability and thus the mean value may not be very relevant. Thus, the results on seasonal variability and even those on cycle comparison should be taken with caution. We noticed in this figure that both curves have similar pattern, with peaks occurring at the same time, except during February and June, where there is a different growth in both cycles. We observe that, the solar flares effects are stronger during March equinox (February-March-April) and September equinox (August-September-October), and weak during June solstice (May-June-July) and December Solstice (November-December-January). On the average, the sfes were stronger in the cycle 23 than the cycle 24. The highest sfe value was recorded in September during both cycles with ΔH_{sfe} = 48.82 nT for cycle 23 and ΔH_{sfe} = 24.68 nT for cycle 24. Conversely, the lowest values of the sfe were registered in June for cycle 23 (ΔH_{sfe} = 8.69 nT) and July for cycle 24 (ΔH_{sfe} = 10.69 nT).

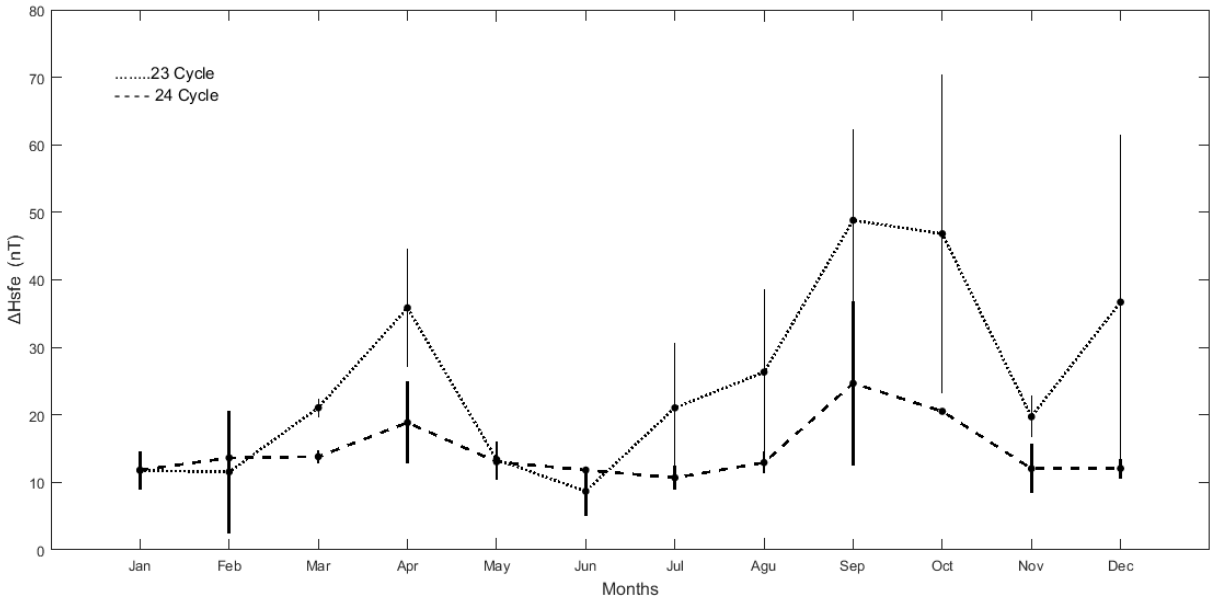

Figure 12. Monthly variations of the sfe during cycles 23 and 24. Points are the average values of each month. The solid line and the dashed line are the average variations of the sfe during cycles 23 and 24, respectively. The error bars are the calculated standard deviations.

4. Discussion

Since the 19th century, meticulous observations of the sun have made it possible to highlight the regularity in the evolution of sunspots. These sunspots are places where formation of the active regions (ARs) responsible for certain solar events such as solar flares (SFs) form. Past studies have shown that there are several ways of classifying solar flares [23]. During periods of strong magnetic activity, a large number of ARs are visible on the sun. The authors of [24] showed that the cyclic variation of sunspots is essentially identical to that of SFs. However, their study did not highlight the variation of sunspots with different classes of SF. In this paper, we made a correlation study between sunspots and each class of SFs. Our results showed that during solar cycles 23 and 24, the number of C and M-class flares were strongly correlated (0.93/0.97 and 0.96/0.96 during SC 23/24 for the respective flare) with sunspot number, while A and B-class correlated negatively with sunspot numbers. This negative correlation between sunspots and classes A and B is due to the fact that both classes of flare are lagged respect the solar cycle. The X-class flares which has a significant impact on the Earth's atmosphere occurred less and correlated moderately with sunspot number (0.60/0.56 during SC23/24). Previous studies have found that more energetic solar flares do not occur frequently on the sun. For example, it has been shown that approximately less than 100 X class solar flares occur every 125,000 years on the surface of the sun [25,26]. However, the authors of [27] revealed that the largest flares (X45 or X50 class) that occur on the visible hemisphere part of the sun can occur at least once per century. We observed that most of the flares that occurred on the surface of the sun did not have a visible magnetic signature on magnetometer recordings at various ground stations. The reasons for this include the fact that these flares occurred during strong magnetic disturbance when the irregular variation of the geomagnetic field components masked the magnetic crochet. The works in [28,29] revealed that other factors, such as poor distribution of observatories around the globe, lack of stations in ocean regions and natural noise, may prevent the observation of magnetic crochets on geomagnetic field component.

Among the 6200 solar flares observed, we studied only 289 most of which corresponded with the solar flares provided by SRMV (http://www.obsebre.es/en/rapid, accessed on 1 November 2021).

The 289 SFs were studied taking into consideration their position on the solar disc (center, transition zone and limb). We notice that the maximum peak of sfe does not always

occur simultaneously at different observatories, and it is more delayed with increasing solar zenith angle in the sunlit hemisphere for some weak sfe. The same results were observed in [9]. It was observed that the sfe produced by the X9.4-class (limb) was smaller than the sfe produce by X6.2-class (center) at the equator. The statistical analysis of the solar flare carried out by [30] showed that a limb flare has a smaller effect than a central flare on the ionosphere. This is due to the EUV absorption in the solar atmosphere. Another factor is the ability of an active region to produce several solar flares as was the case during the two flares of class M1.4 and M4.2, on 30 November 1997. Interestingly, during the successive solar flares of 25 October 2013, some stations experienced stronger sfe during the class X1.7 that occurred at 7:53 UT than the X2.1 one that took place at 14:51 UT. The analysis showed that this case was observed when the effects of the lower-class solar flare were recorded around the local noon time when the H-component usually reached its peak variation. A similar result was obtained at the Millstone Hill station (42.6° N, 71.5° W) by [31]. They studied two solar flares the X8.3-class flare and the X9.3-class flare which occurred at 11:00 LT and 7:00 LT, respectively, from the same active region. They showed that the response of the ionosphere to the solar flare X8.3 was more important than the X9.3-class. The analysis of horizontal component H of the geomagnetic field revealed some important characteristics of solar flares. Thus, we note that the stations around magnetic equator during a flare recorded the highest peak of the magnetic crochet. This is due to the high conductivity of this region due to the equatorial electrojet [32]. Furthermore, we observed an inversion of the magnetic crochets on the H component between mid-latitudes and low latitudes. Generally, the amplitude of the H component was negative in mid-latitudes in both hemispheres and positive in low latitudes. The authors of [20] showed that the reversed sfe appears as a physical consequence of the ionospheric current system geometry and is due to the displacement that the sfe system undergoes in longitude and/or latitude with respect to the sq system. In addition, note that in most of our cases, the amplitude of the magnetic crocket on the H component was inversely proportional to the solar zenith angle. The authors of [31] showed that the position of the solar flare relative to the solar zenith angle and the power of luminance are determining factors in the ionosphere's response to the solar flare. Furthermore, magnetic crochets are not observed synchronously (a few seconds), in stations separated by a short time.

The analysis of the latitudinal variation of the eastward Y and vertical Z components showed that unlike the horizontal H component their patterns of variations were not coherent in latitude. However, the maximum amplitudes of the sfe on the two components (ΔY_{sfe} and ΔZ_{sfe}) were observed in the same stations around the magnetic equator, while lower values were obtained over the northern and southern hemispheric limits. Previous studies in [32] have shown that the variations in ΔY_{sfe} and ΔZ_{sfe} were strongly influenced by the presence of equatorial electrojet and counter electrojet currents around magnetic equator. Similar studies are presented in [33].

In general, the analysis of the variation in latitude of the three components showed a magnetic disturbance appearing as a temporary increase in the diurnal variation of the geomagnetic filed components. The magnetic crochets decreased in amplitude closer to the limits of both sunlit hemisphere and were not observed at night. These peaks were generally stronger for the stations around the magnetic equator and were very low when the geomagnetic field components were close to their night values. Furthermore, it is noted that when a solar flare occurs at a local time close to noon, where the zenith angle is small, the magnetic response was very strong on all geomagnetic components. Such condition favors a strong reaction of the ionosphere to the solar flare and thus, a strong magnetic crochet in stations close to the equator. Studies of the impact of solar zenith angle on SF responses have been conducted in [7,34]. The authors of [7] focused of the sfes on ionospheric absorption with the systematic analysis of ionograms measured at mid-latitude and low-latitude ionosonde stations under different solar zenith angles. [29] analyzed the effect of intense solar flare on TEC variation at low-latitude with and without geomagnetic disturbances, local times effects (solar zenith angle effects) and changing the location of the

solar active region. Both studies showed that the solar zenith angle affects the ionospheric response to solar flare.

Finally, the results of the analysis of the monthly variation of SC 23 and 24 sfe revealed that sfe varied from season to season and from cycle to cycle. The average values obtained from a reduced sample of data show that the ΔH_{sfe} is generally higher in cycle 23 than in cycle 24, which could be justified by the higher level of solar activity characteristic of the last solar cycle. In addition, the average sfe values were higher in the equinoctial month in both solar cycles. In summary, the position of the active region on the sun, the local time, the SZA and the seasonal variations (equinox and solstice seasons), are determining factors in the magnetic response of the components, following a solar flare.

5. Conclusions

In this work we have investigated the effect of SFs on the horizontal (H), eastward (Y) and vertical (Z) components of the earth magnetic field using ground-based magnetometers data during solar cycles 23 and 24 (SC23/24). The relation between sunspot number and solar flare occurrence has also been examined for different flare classes. Our results show that:

(i) The solar flare effect (sfe) was stronger in SC23 than SC24 while equinoctial months had the highest magnetic crochet. The respective highest ΔH_{sfe} values of 48.82 nT and 24.68 nT were obtained in the month of September while the lowest values of 8.69 nT were recorded in June for cycle 23 and 10.69 nT in July for cycle 24.

(ii) C and M-class flares strongly correlated with sunspot number with the respective correlation coefficients of 0.93/0.97, 0.96/0.96 during SC23/24. However, the correlation coefficient for X-class flare was 0.60/0.56.

(iii) The negative correlation between A and B-class flare and sunspot numbers ($-0.43/-0.54$ and $-0.42/-0.39$) during SC23/24 was related to the frequent occurrence of such classes of flare during solar minimum.

(iv) There was a delay of few minutes in the response of the three geomagnetic components to the SFs. Generally, the magnetic crochet of the H component was negative at mid-latitudes in both hemispheres and positive at low-latitudes.

(v) The peak amplitude of the sfe was stronger for the stations around the magnetic equator and very low when the geomagnetic field components were close to their nighttime values.

Author Contributions: Conceptualization, O.D.F.G.; Formal analysis, O.D.F.G.; Supervision, V.D.; Validation, V.D., P.O.A. and C.A.-M.; Visualization, P.O.A., K.N., K.A.A.D., T.Z. and K.B. All authors have read and agreed to the published version of the manuscript.

Funding: This research received no external funding.

Acknowledgments: We thank Intermagnet and the geomagnetic observatories proving the geomagnetic data used in this work. Sincere appreciations to the Geostationary Operational Environmental Satellites (GOES) of the National Oceanic and Atmospheric Administration (NOAA) for the X-ray flux data.

Conflicts of Interest: The authors declare no conflict of interest.

References

1. Le, H.; Liu, L.; Chen, B.; Lei, J.; Yue, X.; Wan, W. Modeling the responses of the middle latitude ionosphere to solar flares. *J. Atmos. Solar-Terr. Phys.* **2007**, *69*, 1587–1598. [CrossRef]
2. Benz, A.O. (Ed.) Astrophysics and Space Science Library. In *Plasma Astrophysics: Kinectic Processes in Solar and Stellar Coronae*; Springer Science & Business Media: Berlin/Heilderbeg, Germany, 1993; Volume 184.
3. Heyvaerts, J. *Recent Developments in Solar Flare Models*; Technical Report N82-85085; NASA Scientific and Technical Information Facility: Washington, DC, USA, 1981.
4. Svestka, Z. *Flare Observation*; Priest, E.R., Ed.; Spinger: Cham, Switzerland, 1981; pp. 47–137.
5. Donnelly, R.F. *SMS-GOES Solar Soft X-Ray Measurements Part, I. sms-1, sms-2 and Goes-1 Measurements from 1 July 1974, through 31 December 1976*; NOAA Technical Memorandum ERL SEL-56; Space Environment Laboratory: Boulder, CO, USA, 1981.

6. Zalnol, N.H.; Hamidi, Z.S.; Shariff, N.N.M.; Marhana, O.A.; Nurulhazwani, H.; Sabri, S.N.U.; Monstein, C. The formation of fundamental structure of solar radio brust type II due X6.9 class solar flare. *WSN* **2016**, *35*, 30–43.
7. Barta, V.; Sátori, G.; Berényi, K.A.; Kis, Á.; Williams, E. Effects of solar flares on the ionosphere as shown by the dynamics of ionograms recorded in Europe and South Africa. *Ann. Geophys.* **2019**, *37*, 747–761. [CrossRef]
8. Wan, W.; Liu, L.; Yuan, H.; Ning, B.; Zhang, S. The GPS measured SITEC caused by the very intense solar flare on 14 July 2000. *Adv. Space Res.* **2005**, *36*, 2465–2469. [CrossRef]
9. Nagata, T. Solar flare on the geomagnetic field. *J. Geomag. Geoelec.* **1996**, *18*, 197–219. [CrossRef]
10. Carrington, R.C. Description of a singular appearance seen in the sun on 1 September 1859. *Mon. Notic. Roy. Astron. Soc.* **1859**, *20*, 13–15. [CrossRef]
11. McNish, A.G. Magnetic Effects associated with Bright Solar Eruptions and Radio Fade-Outs. *Nature* **1937**, *139*, 244. [CrossRef]
12. Rastogi, R.; Kaushika, N.; Trivedi, N. Solar flare crochet and sudden commencement in H within the equatorial electrojet region. *J. Atmos. Terr. Phys.* **1965**, *27*, 663–668. [CrossRef]
13. Pudovkin, M.I.; Babushkina, V.V. Influence of solar flares and disturbances of the interplanetary medium on the atmospheric circulation. *J. Atmos. Terr. Phys.* **1992**, *54*, 841846. [CrossRef]
14. Rao, K.S.R.; Rao, M.P. On the Location of the Ionospheric Current System Causing Geomagnetic Solar Flare Effects. *J. Atmos. Sci.* **1963**, *20*, 498–501. [CrossRef]
15. Rastogi, R.G.; Rangarajan, G.K. Solar Flare in Equatorial magnetic field during morning counter electrojet. *Ind. J. Radio Space Phys.* **1981**, *10*, 190–192.
16. Rastogi, R.G. Effect of solar disturbance on the geomagnetic H, Y and Z fields in American equatorial electrojet stations. *J. Ind. Geophys. Union* **1996**, *7*, 45–53.
17. Rastogi, R.G.; Rangarajan, G.K.; Sen Gupta, A.; Iyer, K.N.; Vyas, G.D. Solar flare of 6 November 1980 and associated ionospheric effects. *Ind. J. Radio Space Phys.* **1983**, *13*, 179–183.
18. Sripathi, S.; Balachandran, N.; Veenadhari, B.; Singh, R.; Emperumal, K. Response of the equatorial and low-latitude ionosphere to an intense X-class solar flare (X7/2B) as observed on 9 August 2011. *J. Geophys. Res. Space Phys.* **2013**, *118*, 2648–2659. [CrossRef]
19. Hamidi, Z.; Abidin, Z.; Ibrahim, Z.; Monstein, C.; Shariff, N.; Sabaghi, M. The Beginning Impulsive of Solar Burst Type IV Radio Emission Detection Associated with M Type Solar Flare. *Int. J. Fundam. Phys. Sci.* **2012**, *2*, 29–31. [CrossRef]
20. Curto, J.J.; Amory-Mazaudier, C.; Torta, J.M.; Menvielle, M. Solar flare effects at Ebre: Regular and reversed solar flare effects, statistical analysis (1953 to 1985), A global case study and a model of elliptical ionospheric currents. *J. Geophys. Res. Space Phys.* **1994**, *99*, 3945–3954. [CrossRef]
21. Taat, A.; Abbas, M.; Jusoh, M.H. The Response of Geomagnetic H and Z Components During X-Class Solar Flare. *J. Phys. Conf. Ser.* **2019**, *1152*, 012031. [CrossRef]
22. Dmitriev, A.V.; Yeh, H.C. Geomagnetic signatures of sudden ionospheric disturbances during extreme solar radition events. *J. Atmos. Sol. Terr. Phys.* **2008**, *70*, 1971–1984. [CrossRef]
23. Bai, T.; Sturrock, P.A. *Classification of Solar Flares*; Defense Technical Information Center: Fort Belvoir, VA, USA, 1988. [CrossRef]
24. Fröhlich, C. Evidence of a long-term trend in total solar irradiance. *Astron. Astrophys.* **2009**, *501*, L27–L30. [CrossRef]
25. Maehara, H.; Shibayama, T.; Notsu, S.; Notsu, Y.; Nagao, T.; Kusaba, S.; Honda, S.; Nogami, D.; Shibata, K. Superflares on solar-type stars. *Nature* **2012**, *485*, 478–481. [CrossRef] [PubMed]
26. Shibata, K.; Isobe, H.; Hillier, A.; Choudhuri, A.R.; Maehara, H.; Ishii, T.T.; Shibayama, T.; Notsu, S.; Notsu, Y.; Nagao, T.; et al. Can Superflares Occur on Our Sun? *Publ. Astron. Soc. Jpn.* **2013**, *65*. [CrossRef]
27. Curto, J.J.; Castell-Queralt, J.; Del Moral, F. Sfe: Waiting for the big one. *J. Space Weather Space Clim.* **2016**, *6*, A23. [CrossRef]
28. Curto, J.J.; Gaya-Piqué, L.R. Geoeffectiveness of solar flares in magnetic crochet (sfe) production: II—Dependence on the detection method. *J. Atmos. Solar-Terr. Phys.* **2009**, *71*, 1705–1710. [CrossRef]
29. Curto, J.J. Geomagnetic solar flare effects: A review. *J. Space Weather Space Clim.* **2020**, *10*, 27. [CrossRef]
30. Le, H.; Liu, L.; Chen, Y.; Wan, W. Statistical analysis of ionospheric responses to solar flares in the solar cycle 23. *J. Geophys. Res. Space Phys.* **2013**, *118*, 576–582. [CrossRef]
31. Qian, L.; Wang, W.; Burns, A.G.; Chamberlin, P.C.; Coster, A.; Zhang, S.-R.; Solomon, S.C. Solar flare and geo-magnetic storm effects on the thermosphere and ionosphere during 6–11 September 2017. *J. Geophys. Res. Space Phys.* **2019**, *124*, 2298–2311. [CrossRef]
32. Rastogi, R.G.; Pathan, B.M.; Rao, D.R.K.; Sastry, T.S.; Sastri, J.H. Solar flare effects on the geomagnetic elements during normal and counter electrojet periods. *Earth Planets Space* **1999**, *51*, 947–957. [CrossRef]
33. Annadurai, N.M.N.; Hamid, N.S.A.; Yamazaki, Y.; Yoshikawa, A. Investigation of Unusual Solar Flare Effect on the Global Ionospheric Current System. *J. Geophys. Res. Space Phys.* **2018**, *123*, 8599–8609. [CrossRef]
34. Singh, A.; Rao, S.S.; Rathore, V.S.; Singh, S.K.; Singh, A.K. Efeect of intense solar flare on TEC variation at low-latitude station Varanasi. *J. Astrophys. Astr.* **2020**, *41*, 19. [CrossRef]